# Antisymmetric thermopolarization by electric toroidicity

Joji Nasu [1,2] and Satoru Hayami [3,2,4]
[1]*Department of Physics, Tohoku University, Sendai 980-8578, Japan*
[2]*PRESTO, Japan Science and Technology Agency, Honcho Kawaguchi, Saitama 332-0012, Japan*
[3]*Department of Applied Physics, The University of Tokyo, Tokyo 113-8656, Japan*
[4]*Faculty of Science, Hokkaido University, Sapporo 060-0810, Japan*

(Received 12 December 2021; revised 17 February 2022; accepted 6 June 2022; published 17 June 2022)

We investigate electric polarizations that emerge perpendicular to an applied thermal gradient in insulating systems. The thermally induced electric polarization, known as thermopolarization, has been studied conventionally in the case where an electric polarization appears along the thermal gradient. Here, we focus on the antisymmetric component of the thermopolarization tensor, and we reveal that it becomes nonzero due to the ferrotype order for electric-toroidal dipole moments. To describe local electric polarizations originating from the disproportionation of localized electronic clouds, we introduce a two-dimensional three-orbital model with localized $s$ and two $p$ orbitals, where the electric polarization at each site interacts with the neighboring one as dipole-dipole interactions. We find that a vortex-type configuration of local electric polarizations appears as a mean-field ground state, corresponding to a ferrotype electric-toroidal dipole order. By taking account of collective modes from this ordered state, we calculate the coefficient of the thermopolarization based on the linear-response theory. The antisymmetric component is nonzero in the presence of the electric-toroidal dipole order. We clarify that fluctuations in the $p$ orbitals are crucial in enhancing the antisymmetric thermopolarization. We discuss the appearance conditions based on the symmetry argument and the relevance to real materials.

DOI: 10.1103/PhysRevB.105.245125

## I. INTRODUCTION

The study of cross-correlations in condensed-matter physics has a long history since the discovery of the magnetoelectric effect in $Cr_2O_3$ [1–4]. Even now, the coupling between quantities with distinct symmetries has attracted considerable attention in the fields of strongly correlated electron systems and multiferroics as it strongly reflects the nature of symmetry breaking [5–10]. While most of the studies have focused on the coupling between electricity and magnetism, other properties such as elastic and thermal properties are also expected to contribute to cross-correlations. For example, the thermal gradient trivially induces a thermal current in the system, but it can also generate an electric polarization and magnetization in systems with particular symmetries [11–15]. The thermally induced electric polarization is known as thermopolarization [16–26], where the difference of the temperatures at two opposite edges yields disproportionation of electronic clouds or lattice positions, and thereby a macroscopic electric polarization appears in the system. In this case, it is natural to consider that the direction of the electric polarization is parallel to that of the thermal gradient. Nevertheless, one cannot exclude the possibility of the emergent polarization perpendicular to the thermal gradient, which is an anomalous contribution whose response tensor is not only off-diagonal but also antisymmetric, similar to the Hall effect.

To elucidate in what cases cross-correlation occurs, multipole-based research has developed [27–30]. It tells us the necessary conditions for the emergence of a cross-correlation response based on the symmetries of the lattice geometry, electronic structure, and order parameter. Among them, toroidal-type orders have recently attracted increasing interest [10,27,31,32]. In particular, a magnetic-toroidal dipole moment is crucial for magnetoelectric effects because it is odd for both time and spatial reversal operations. The electric counterpart of the magnetic-toroidal multipoles can also be introduced; they are referred to as electric-toroidal multipoles [33–37]. The multipoles are given by the time-reversal even and axial tensors. Recently, it was pointed out that the bond-length modulation emergent in the pyrochlore oxide $Cd_2Re_2O_7$ [38–49] can be interpreted as an electric-toroidal quadrupole order, which is spatial (time) reversal parity-odd (-even) [50,51]. Nonetheless, an electronic order involving the electric-toroidal dipoles, simpler than the quadrupole ones, remains elusive. This is because the dipole component is both spatial and time-reversal parity-even, complicating its experimental observation, while the longitudinal dissipationless spin-current generation was proposed recently, originating from electric-toroidal octupoles [52].

On the other hand, an electric-toroidal dipole order caused by lattice distortions has been studied as a ferroaxial order [35]. The ferroaxial (ferrorotational) order was initially introduced as a ferrotype order described by an axial vector without the time and spatial symmetry breakings. Recently, an attempt was made to observe the domains of the ferroaxial order by light. In the ferroaxial order, the mirror symmetry is preserved on the plane perpendicular to the ordering vector. Once the electric field parallel to this vector breaks the

 

mirror symmetry, a chirality appears in the system. The optical rotation can identify the direction [53]. This scheme directly observes the chirality induced by the electric field rather than the electric-toroidal dipole order. Moreover, a ferroaxial order was also observed by using the second-harmonic generation via its electric quadrupole component [54]. Therefore, the direct observation of the electric-toroidal dipole is desired as a linear response. However, this is not expected to couple linearly with electric and magnetic fields.

In this paper, we propose that the thermal response can be an appropriate probe to observe the electric-toroidal dipole originating from electronic orbitals. We introduce a three-orbital model with localized $s$ and two $p$ orbitals capable of generating an electric polarization. To consider the electric order of the local polarizations constituting a ferrotype electric-toroidal dipole configuration, we define the model Hamiltonian on a square-octagon lattice. This is one of the simplest lattice structures to stabilize the electric-toroidal dipole order induced by the dipole-dipole interaction. We examine the three-orbital model using the mean-field approximation, and we calculate the thermal response by applying excitation-wave theory. The ferrotype electric-toroidal dipole order appears when the energy gap between the $s$ and $p$ orbitals is small compared with the energy scale of the dipole-dipole interaction. We find that the macroscopic polarization appears perpendicular to the applied thermal gradient, and its linear response coefficient is antisymmetric for their directions. This effect is regarded as an antisymmetric thermopolarization, which is an intrinsic one unrelated to the relaxation time of the thermal transport. We also clarify that the thermopolarization is strongly enhanced when the $p$ orbital level is lower than the $s$ orbital one. This implies that fluctuations on the two $p$ orbitals play a crucial role in enhancing the thermopolarization. We demonstrate the presence of the fluctuations by calculating the excitation spectrum, in which the low-energy excitations changing the direction of the local electric moment exist. We also discuss the relevance to real materials and the origin of the antisymmetric thermopolarization based on the symmetry argument.

This paper is organized as follows. In the next section, we introduce a three-orbital model on a two-dimensional lattice with local electric dipole moments. The method used in this study is presented in Sec. III. In Sec. III A, we describe the mean-field theory applied to the model Hamiltonian and the way to address the fluctuations from the mean fields as elementary excitations. The formulation of the thermopolarization is given in Sec. III B. The results are shown in Sec. IV. In Sec. IV A, we present the mean-field results where the electric-toroidal dipole order appears when the orbital level splitting is small compared with the dipole-dipole interactions. We also show that the antisymmetric thermopolarization emerges in the electric-toroidal dipole ordered phase in Sec. IV B. In Sec. IV C, we show the elementary excitations, which are crucial for the emergence of the nonzero thermopolarization. In Sec. V, we discuss the relevance to real materials and the origin of the antisymmetric thermopolarization from the viewpoint of the symmetry. Finally, Sec. VI is devoted to the summary.

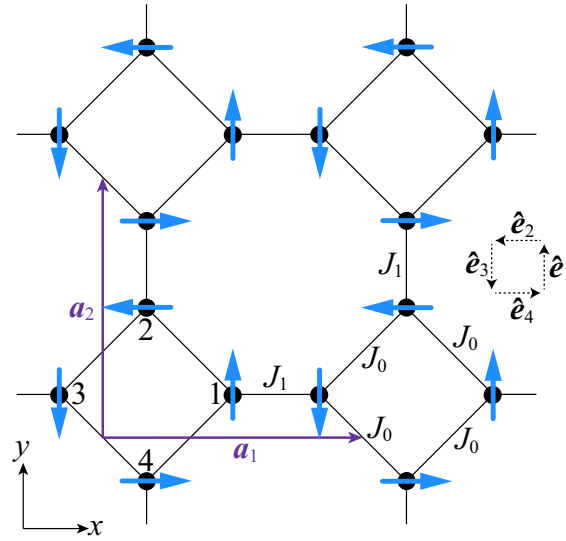


FIG. 1. Schematic figure of the two-dimensional square-octagon lattice. The vectors $\boldsymbol{a}_1$ and $\boldsymbol{a}_2$ shown in purple represent primitive translational vectors, and there are four sites in a unit cell. The blue arrows stand for the local electric polarizations arranged with a toroidal-type configuration. The inset on the right side shows the four unit vectors, each of which is parallel to the blue arrow located on the corresponding site.

## II. MODEL

We introduce a simple model with local electric dipole moments to address the thermopolarization induced by the electric-toroidal dipole moment. We consider three states—$s$, $p_x$, and $p_y$ orbitals—at each site on a two-dimensional square-octagon lattice, where the edges of neighboring squares are connected by lines as shown in Fig. 1. Using these states, the local electric dipole moment on the $xy$ plane is given by $\boldsymbol{P}_i = (P_i^x, P_i^y)$, with $P_i^\gamma \propto |s\rangle_i\langle p_\gamma|_i + \text{H.c.}$ $(\gamma = x, y)$. Here, we assume that the constant of the proportionality is 1, namely, the elementary electric charge $e$ is regarded as unity in addition to the reduced Planck constant $\hbar$, the Boltzmann constant $k_B$, and the length of the primitive translational vectors. The electric dipoles interact as the dipole-dipole interaction. The dominant contributions come from interactions on nearest-neighbor bonds, which are given by

$$\mathcal{H}_{\text{int}} = \sum_{\langle ij \rangle} J_{ij}[\boldsymbol{P}_i \cdot \boldsymbol{P}_j - 3(\boldsymbol{P}_i \cdot \boldsymbol{e}_{ij})(\boldsymbol{P}_j \cdot \boldsymbol{e}_{ij})], \tag{1}$$

where $\langle ij \rangle$ stands for neighboring sites connected by the vector $\boldsymbol{e}_{ij}$ on the bonds of the square-octagon lattice, and $J_{ij} = J_0$ $(J_1)$ for the intrasquare (intersquare) interaction, which is positive (see Fig. 1). In addition to the dipole-dipole interaction, we consider the energy difference $\Delta$ between the $s$ and $p$ orbitals, and the local anisotropy, where the energy level of the $p$ orbital spread along the direction to the center of the square to which the site belongs is higher than the perpendicular orbital by $A$ $(> 0)$. We refer to the former (latter) $p$ orbital as $|p_\perp\rangle$ $(|p_\parallel\rangle)$. These contributions are written as

$$\mathcal{H}_{\text{loc}} = \sum_i [(\Delta + A)|p_\perp\rangle_i\langle p_\perp|_i + \Delta|p_\parallel\rangle_i\langle p_\parallel|_i]. \tag{2}$$

The model Hamiltonian $\mathcal{H} = \mathcal{H}_{\rm int} + \mathcal{H}_{\rm loc}$ is expected to exhibit the electric-toroidal dipole moment in a unit cell shown in Fig. 1 within the nearest-neighbor interactions. If this electric-polarization configuration is present, the first (second) term in Eq. (1) disappears on the intrasquare (intersquare) bonds, and the ferrotype (antiferrotype) contribution survives, which stabilizes the assumed configuration in addition to the positive anisotropy $A$. Thus, we believe that the present Hamiltonian provides a simple and appropriate model to discuss the effect of electric-toroidal dipole moments.

## III. METHOD

### A. Mean-field theory and elementary excitations

To examine the electric-toroidal dipole order appearing in the Hamiltonian, we apply the mean-field approximation and linear excitation-wave theory. The present system is similar to that with quantum paraelectricity, which has been discussed using the transverse Ising model [55–57]; in this study, $\mathcal{H}_{\rm loc}$ is regarded as a transverse field because the local electric moment describes the mixing of the $s$ and $p$ orbitals. One of the simplest ways to deal with the dynamics of the high-dimensional transverse Ising model is the linear excitation-wave approximation introduced later, and we apply this method to the present model.

The dipole-dipole interaction is symbolically written as

$$\mathcal{H}_{\rm int} = \sum_{\langle ij\rangle}\sum_{\gamma\gamma'} J_{ij}^{\gamma\gamma'} P_i^{\gamma} P_j^{\gamma'}. \tag{3}$$

The mean-field approximation applied to it gives

$$\mathcal{H}_{\rm int}^{\rm MF} = \sum_{\langle ij\rangle}\sum_{\gamma\gamma'} J_{ij}^{\gamma\gamma'} \left(\langle P_i^{\gamma}\rangle P_j^{\gamma'} + P_i^{\gamma}\langle P_j^{\gamma'}\rangle - \langle P_i^{\gamma}\rangle\langle P_j^{\gamma'}\rangle\right), \tag{4}$$

where the different mean fields are prepared for four sublattice sites ($M = 4$) in the unit cell of the square-octagon lattice (see Fig. 1). We determine the mean fields $\langle P_i^{\gamma}\rangle$ by solving the single-site Hamiltonian $\mathcal{H}_i^{\rm MF}$ in $\mathcal{H}^{\rm MF} = \mathcal{H}_{\rm int}^{\rm MF} + \mathcal{H}_{\rm loc}$, and the expectation value is calculated for the ground state of $\mathcal{H}_i^{\rm MF}$, $|0\rangle_i$.

Next, we introduce the linear excitation-wave theory. The deviation from the mean-field Hamiltonian is written as

$$\mathcal{H}' = \mathcal{H}_{\rm int} - \mathcal{H}_{\rm int}^{\rm MF} = \sum_{\langle ij\rangle}\sum_{\gamma\gamma'} J_{ij}^{\gamma\gamma'} \delta P_i^{\gamma} \delta P_j^{\gamma'}, \tag{5}$$

where $\delta P_i^{\gamma} = P_i^{\gamma} - \langle P_i^{\gamma}\rangle$. In the linear excitation-wave theory, $\delta P_i^{\gamma}$ is approximated by extracting the matrix elements involving the ground state of $\mathcal{H}_i^{\rm MF}$ as [58–64]

$$\delta P_i^{\gamma} \simeq \sum_{m=1,2} a_{im}^{\dagger} \langle m|_i \delta P_i^{\gamma} |0\rangle_i + \text{H.c.}, \tag{6}$$

where $|m\rangle_i$, with $m = 1, 2$, is the excited state of the local mean-field Hamiltonian $\mathcal{H}_i^{\rm MF}$ at site $i$, and $a_{mi}^{\dagger} = |m\rangle_i\langle 0|_i$ is assumed to be a creation operator of a boson, corresponding to the Holstein-Primakoff quasiparticle. Applying this approximation, we rewrite the Hamiltonian as a bilinear form of the bosonic operators:

$$\mathcal{H} \simeq \tilde{\mathcal{H}} = \frac{1}{2}\sum_{\boldsymbol{k}ll'} H_{\boldsymbol{k}ll'} \mathcal{A}_{\boldsymbol{k}l}^{\dagger} \mathcal{A}_{\boldsymbol{k}l'}, \tag{7}$$

where $\mathcal{A}_{\boldsymbol{k}}^{\dagger} = (a_{\boldsymbol{k}1}^{\dagger}, \ldots, a_{\boldsymbol{k},2M}^{\dagger}, a_{-\boldsymbol{k}1}, \ldots, a_{-\boldsymbol{k},2M})$ whose element is assigned by $l = 1, 2, \ldots, 4M$, and $a_{\boldsymbol{k}(s,m)}^{\dagger} = \sqrt{M/N}\sum_{i\in s} a_{im}^{\dagger} e^{i\boldsymbol{k}\cdot\boldsymbol{r}_i}$ for sublattice $s$. The $4M \times 4M$ matrix $H_{\boldsymbol{k}}$ is diagonalized by the Bogoliubov transformation with the paraunitary matrix $T_{\boldsymbol{k}}$ as [65]

$$\tilde{\mathcal{H}} = \frac{1}{2}\sum_{\boldsymbol{k}n} \mathcal{E}_{\boldsymbol{k}n} \mathcal{B}_{\boldsymbol{k}n}^{\dagger} \mathcal{B}_{\boldsymbol{k}n} + \text{const}, \tag{8}$$

where $\mathcal{E}_{\boldsymbol{k}} = (\varepsilon_{\boldsymbol{k}1}, \ldots, \varepsilon_{\boldsymbol{k},2M}, \varepsilon_{-\boldsymbol{k}1}, \ldots, \varepsilon_{-\boldsymbol{k},2M})$ and $\mathcal{B}_{\boldsymbol{k}}^{\dagger} = (b_{\boldsymbol{k}1}^{\dagger}, \ldots, b_{\boldsymbol{k},2M}^{\dagger}, b_{-\boldsymbol{k}1}, \ldots, b_{-\boldsymbol{k},2M}) = \mathcal{A}_{\boldsymbol{k}}^{\dagger} T_{\boldsymbol{k}}^{-1\dagger}$. The paraunitary matrix satisfies the following equation:

$$T_{\boldsymbol{k}} \mathcal{I} T_{\boldsymbol{k}}^{\dagger} = T_{\boldsymbol{k}}^{\dagger} \mathcal{I} T_{\boldsymbol{k}} = \mathcal{I}, \tag{9}$$

where $\mathcal{I}$ is the paraunit matrix, which is diagonal and defined such that $\mathcal{I}_{nn} = \mathcal{I}_n = +1$ for $n \leqslant 2M$ and $\mathcal{I}_n = -1$ for $n > 2M$.

### B. Formalism of thermopolarization

Here, we introduce the coefficient of the off-diagonal thermopolarization, $\beta^{xy}$, defined as

$$\frac{\langle P^x\rangle_{\nabla_y T}}{V} = \beta^{xy}(-\nabla_y T), \tag{10}$$

where $\langle P^x\rangle_{\nabla_y T}$ stands for the polarization under the thermal gradient, and $V$ is the volume. When the thermal gradient is absent, the averaged macroscopic polarization $\langle P^x\rangle$ becomes zero, i.e., $\langle P^x\rangle = 0$ in equilibrium because of the toroidal-type configuration of the local electric polarizations shown in Fig. 1. Since $P^x$ should vanish without bosonic excitations, the total polarization is approximately written as a bilinear form of the bosons:

$$P^x = \sum_i P_i^x \simeq \frac{1}{2}\sum_{\boldsymbol{k}nn'} \mathcal{P}_{\boldsymbol{k}nn'}^x \mathcal{B}_{\boldsymbol{k}n}^{\dagger} \mathcal{B}_{\boldsymbol{k}n'}, \tag{11}$$

where $\mathcal{P}_{\boldsymbol{k}}^x$ is a $4M \times 4M$ Hermitian matrix. The velocity matrix is given by

$$\mathcal{V}_{\boldsymbol{k}}^y = T_{\boldsymbol{k}}^{\dagger} \frac{\partial H_{\boldsymbol{k}}}{\partial k_y} T_{\boldsymbol{k}}. \tag{12}$$

Using these quantities, the coefficient $\beta^{xy}$ is represented as [66–68]

$$\beta^{xy} = -\frac{1}{V}\sum_{\boldsymbol{k}}\sum_{n=1}^{2M} c_1(n(\varepsilon_{\boldsymbol{k}n}))\Omega_{\boldsymbol{k}n}^{xy}, \tag{13}$$

where the temperature-independent part $\Omega_{\boldsymbol{k}n}^{xy}$ is given by

$$\Omega_{\boldsymbol{k}n}^{xy} = -2\sum_{n'(\neq n)}^{4M} \frac{\mathrm{Im}[\mathcal{P}_{\boldsymbol{k}nn'}^x \mathcal{V}_{\boldsymbol{k}n'n}^y]\mathcal{I}_n\mathcal{I}_{n'}}{(\mathcal{I}_n\varepsilon_{\boldsymbol{k}n} - \mathcal{I}_{n'}\varepsilon_{\boldsymbol{k}n'})^2}. \tag{14}$$

The temperature dependence of $\beta^{xy}$ originates from its coefficient $c_1(n(\varepsilon_{\boldsymbol{k}n}))$, where $n(\varepsilon) = (e^{\varepsilon/T} - 1)^{-1}$ is the Bose distribution function, and

$$c_1(x) = (1 + x)\ln(1 + x) - x\ln x. \tag{15}$$

We only consider the antisymmetric part, i.e., $\beta^{xy} = -\beta^{yx}$, which is an intrinsic contribution independent of the relaxation time, because the off-diagonal symmetric part should

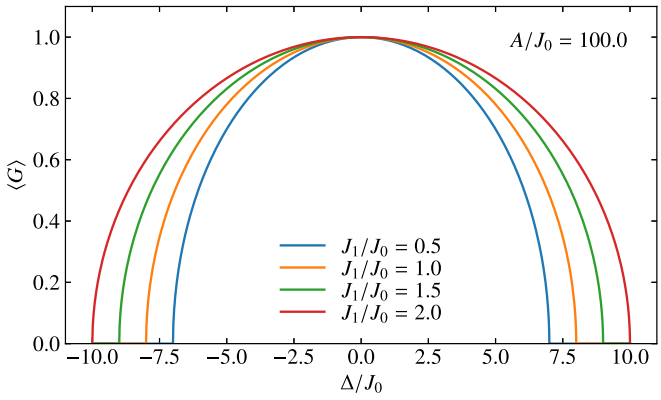


FIG. 2. $\Delta$ dependence of the order parameter of the toroidal-type configuration for the electric dipole moments at $A/J_0 = 100$.

vanish for the toroidal-type configuration shown in Fig. 1 with $C_4$ symmetry.

## IV. RESULT

### A. Electric-toroidal dipole order

First, we show the mean-field results at zero temperature. In the present calculations, we only find the toroidal-type electric dipole order depicted in Fig. 1, as expected. The order parameter is given by

$$\langle G \rangle = \frac{1}{N} \sum_{p=1,2,3,4} \hat{\boldsymbol{e}}_p \cdot \sum_{i \in p} \langle \boldsymbol{P}_i \rangle, \tag{16}$$

where we define the following unit vectors: $\hat{\boldsymbol{e}}_1 = (0, 1)$, $\hat{\boldsymbol{e}}_2 = (-1, 0)$, $\hat{\boldsymbol{e}}_3 = (0, -1)$, and $\hat{\boldsymbol{e}}_4 = (1, 0)$ (see the inset of Fig. 1). Figure 2 shows the $\Delta$ dependence of $\langle G \rangle$ for several values of $J_1$ at $A/J_0 = 100$. This quantity is nonzero around $\Delta = 0$, indicating the electric-toroidal dipole order, and it continuously decreases and becomes zero by increasing $|\Delta|$. As discussed in Sec. III A, the present model is similar to the transverse Ising model. For the case of large anisotropy, the local $s$ and $p_\parallel$ orbitals with the energy difference $\Delta$ dominate the low-energy properties, and nonzero $\langle G \rangle$ is a consequence of the mixing between these orbitals. The symmetric and domelike behavior of $\langle G \rangle$ as a function of $\Delta$ is understood as an analogy of the transverse Ising model. The thermopolarization in this model on the zigzag chain is discussed in Appendix.

As shown in Fig. 2, the region of the electric-toroidal dipole order becomes large with increasing $J_1$. The critical value of $\Delta$ is given by $\Delta_c = 6J_0 + 2J_1$, which is understood from the magnitude of the mean field yielded by the electric dipoles surrounding a certain site. Note that $\Delta_c$ is independent of the local anisotropy $A$. To confirm this clearly, we show the $A$ dependence of the order parameter $\langle G \rangle$ in Fig. 3(a). In this figure, $\langle G \rangle$ as a function of $\Delta$ is presented for several values of $A$, but all the lines appear to overlap with each other. This result indicates that the anisotropy does not affect the phase boundary and the $\Delta$ dependence of $\langle G \rangle$ even for small $A$.

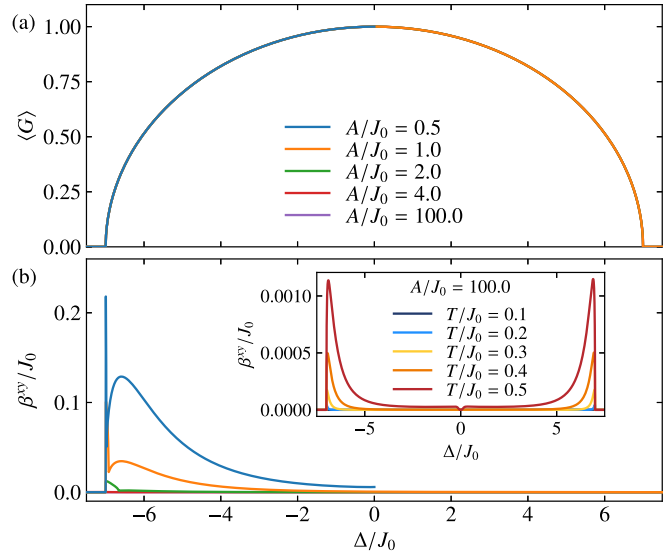


FIG. 3. (a) Toroidal order parameter and (b) the coefficient of the thermopolarization, $\beta^{xy}$, as functions of $\Delta$ for several $A$. In (b), the temperature is set at $T/J_0 = 0.3$. The inset of (b) shows the $\Delta$ dependence of $\beta^{xy}$ for several temperatures at $A/J_0 = 100$. $J_1/J_0$ is fixed to 0.5. We show the data only for the region where the ground state is stable against the creation of elementary excitations.

### B. Thermopolarization

Although the ground-state phase diagram remains largely intact for the anisotropy, it is expected to change the excitation spectra. The low-energy excitations from the ground state contribute to the transport phenomena. In particular, we focus on the off-diagonal thermopolarization, which was introduced in the previous section. Figure 3(b) shows the $\Delta$ dependence of the coefficient $\beta^{xy}$ for several $A$ at $T/J_0 = 0.3$. As shown in this figure, $\beta^{xy}$ is almost zero at $A/J_0 = 100$, but it increases with decreasing $A$. We find that $\beta^{xy}$ takes a large value near the critical point in the region of negative $\Delta$. Note that the $\Delta$ dependence of $\beta^{xy}$ shown in Fig. 3(b) appears to be uncorrelated with that of $\langle G \rangle$ in Fig. 3(a) at first glance. This is due to the contribution from the excitation structure depending on $\Delta$. The coefficient of antisymmetric thermopolarization, $\beta^{xy}$, is considered to be approximately proportional to the product of the electric-toroidal dipole moment and the function of the excitation structure. We can see this relationship in the simpler model given in Appendix as Eq. (A16).

The enhancement around the critical point of $\Delta$ is also observed in the temperature dependence. As shown in Fig. 4, $\beta^{xy}$ increases with increasing temperature and takes a large value when $\Delta$ approaches the critical value $-\Delta_c = -7J_0$ for $A/J_0 = 1$. In particular, at $\Delta/J_0 = -6.99$, $\beta^{xy}$ grows around $T/J_0 = 0.12$, which is lower than the temperatures in the other cases. This suggests that the enhancement of $\beta^{xy}$ around the critical region originates from the small gap in the low-energy excitations. On the other hand, around the critical point in the positive $\Delta$, the enhancement of $\beta^{xy}$ is not observed even for small $A$ [$\beta^{xy}$ is almost zero for $\Delta > 0$ at $A/J_0 = 1$, as shown in Fig. 3(b)]. The asymmetry is due to the presence of the $p$ orbital degeneracy; the local level of the doubly degenerate $p$ orbitals is lower than that of the $s$ orbital for $\Delta < 0$ at $A = 0$,

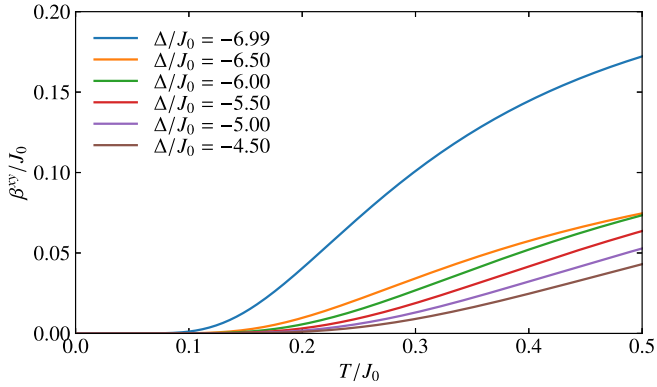


FIG. 4. Temperature dependence of the coefficient of the thermopolarization at $J_1/J_0 = 0.5$ and $A/J_0 = 1$.

but the nondegenerate $s$ orbital is the local ground state for $\Delta > 0$.

To examine the impact of the fluctuating $p$ orbitals on enhancing the thermopolarization, we introduce a simple transverse Ising model on a zigzag chain, $\mathcal{H}_{\rm TI}$ (see the details in Appendix). There are two local states at each site in this model, unlike the present Hamiltonian with three local states. We find that the coefficient of the off-diagonal thermopolarization is symmetric for the transverse field as well as the order parameter in the transverse Ising model (Fig. 9). This is in stark contrast to the present three-orbital model with small $A$, as shown in the main panel of Fig. 3(b). Moreover, the absolute value of the coefficient in the transverse Ising model is significantly small compared with the energy scale of the interaction, even in the vicinity of the critical points. Indeed, similar behavior is observed in the three-orbital model with large anisotropy, regarded as a two-orbital model like the transverse Ising model. The inset of Fig. 3(b) shows $\beta^{xy}$ for $A/J_0 = 100$ at several temperatures. The symmetric $\Delta$ dependence and the order of the peak value around the critical points appear to be common to those of the transverse Ising model. These results indicate that the $p$ orbitals play an essential role in enhancing the thermopolarization.

### C. Elementary excitation spectrum

The effect of the fluctuating $p$ orbitals can be clarified by examining the excitation spectrum from the ground state. Figure 5 shows the dispersion relations $\varepsilon_{\boldsymbol{k}n}$ of the collective modes and contributions from the corresponding branch to the thermopolarization, $\Omega^{xy}_{\boldsymbol{k}n}$. The dispersion relations for the small and large values of the anisotropy at $\Delta/J_0 = -6$ are presented in Figs. 5(a) and 5(b), respectively. At $A/J_0 = 1$, there are four high-energy branches above $3J_0$ and low-energy excitations below $2J_0$ with small dispersions. The former are almost unchanged by the large anisotropy, but the latter disappear in the case with $A/J_0 = 100$, which are located around the higher-energy region scaled by $A$. These results indicate that the four dispersive branches around $6J_0$ are interpreted as longitudinal modes varying the amplitude of the electric dipoles, which originate from transitions between the $s$ and $p$ orbitals. This contribution is insensitive to the anisotropy because the

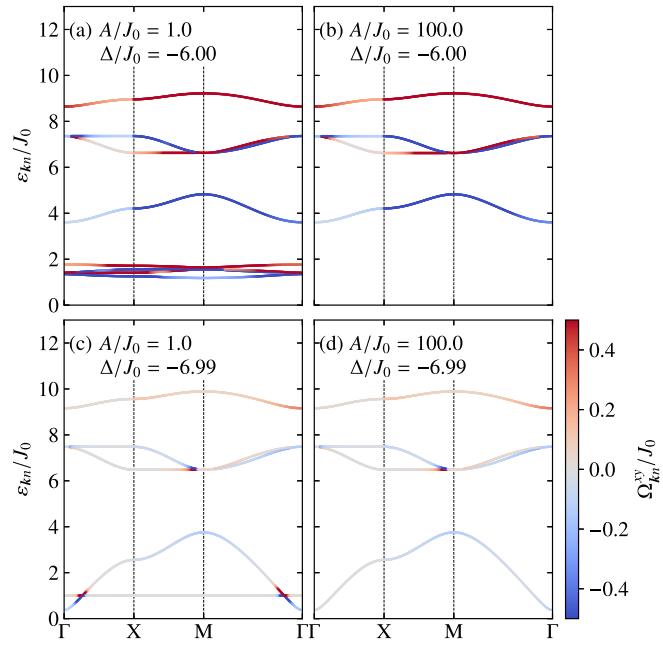


FIG. 5. (a),(b) Dispersion relations of the collective modes from the toroidal-type electric dipole order for (a) $A/J_0 = 1$ and (b) $A/J_0 = 100$ at $\Delta/J_0 = -6$. The color of the lines represents the value of $\Omega_{\boldsymbol{k}n}$ for the corresponding excitation. (c),(d) Corresponding plots for $\Delta/J_0 = -6.99$. $J_1/J_0$ is fixed to 0.5. The wave-vector points $X$ and $M$ denote $\boldsymbol{k} = (\pi, 0)$ and $(\pi, \pi)$, respectively.

local level splitting between the $s$ and $p_\parallel$ is independent of $A$.

On the other hand, the anisotropy $A$ lifts the degeneracy of the local $p$ orbitals and yields the energy splitting between the $p_\parallel$ and $p_\perp$ orbitals. Since the energy gap of the low-energy modes below $3J_0$ in Fig. 5(a) depends on the anisotropy $A$, these modes are understood as the fluctuation between the two orbitals, corresponding to the transverse modes changing the direction of the electric dipoles. The low-energy transverse modes are associated with nonzero $\Omega^{xy}_{\boldsymbol{k}n}$, which leads to a significant value of $\beta^{xy}$ compared to that in the case with the large local anisotropy. Moreover, we also find the negative $\Omega^{xy}_{\boldsymbol{k}n}$ in the lowest energy branch in Fig. 5(a). This results in a positive value of $\beta^{xy}$ because of the negative sign in Eq. (13).

Next, we focus on the vicinity of the critical point at $\Delta/J_0 = -7$. Figure 5(c) shows the excitation spectrum at $\Delta/J_0 = -6.99$ and $A/J_0 = 1$. In this case, there are four almost nondispersive branches at $\simeq J_0$, which are transverse modes. This energy corresponds to the value of the anisotropy $A$, and these branches are not observed at $A/J_0 = 100$ in the energy window of Fig. 5(d). We find that the averaged value of $\Omega^{xy}_{\boldsymbol{k}n}$ for the transverse modes at $A/J_0 = 1$ is almost zero, and hence these modes have only a limited effect on $\beta^{xy}$. However, around the crossing points between the transverse and longitudinal modes, $\Omega^{xy}_{\boldsymbol{k}n}$ takes a large value. The low-energy transverse modes yield this effect as it is not observed in Fig. 5(d). In particular, $\Omega^{xy}_{\boldsymbol{k}n}$ for the low-energy longitudinal mode below $\varepsilon/J_0 \sim 1$ takes a considerable negative value due to the suppression of the denominator value in Eq. (14), which

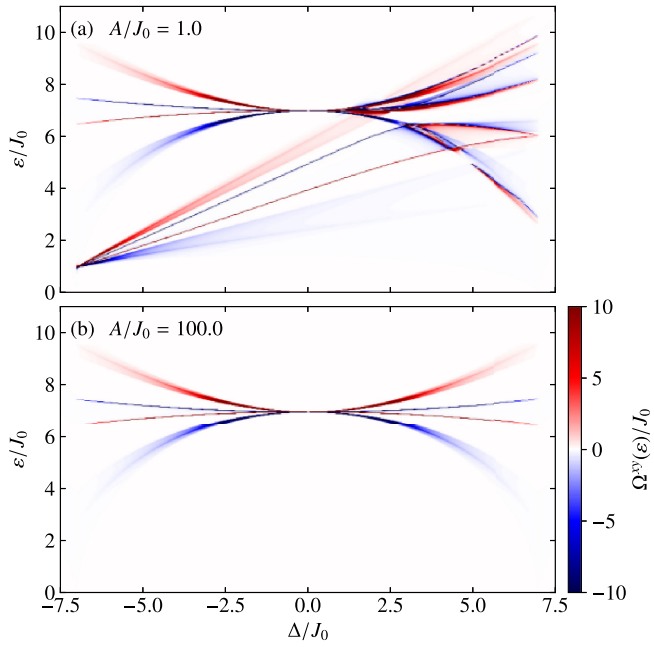


FIG. 6. Contour map of $\Omega^{xy}(\varepsilon)$ on the plane of $\Delta$ and $\varepsilon$ for $A/J_0 = 1$ and $A/J_0 = 100$. $J_1/J_0$ is fixed to 0.5.

results in a substantial enhancement of the thermopolarization in the vicinity of the critical point.

To see this effect more clearly, we calculate the $\Delta$ dependence of the density of $\Omega^{xy}_{\boldsymbol{k}n}$, which is temperature-independent and defined as

$$\Omega^{xy}(\varepsilon) = \frac{1}{V}\sum_{\boldsymbol{k}}\sum_{n=1}^{2M}\Omega^{xy}_{\boldsymbol{k}n}\delta(\varepsilon - \varepsilon_{\boldsymbol{k}n}). \tag{17}$$

Using this spectral representation, the coefficient of thermopolarization is given as

$$\beta^{xy} = -\int c_1(n(\varepsilon))\Omega^{xy}(\varepsilon)d\varepsilon. \tag{18}$$

Figures 6(a) and 6(b) show the $\Delta$ dependence of $\Omega^{xy}(\varepsilon)$ at $A/J_0 = 1$ and 100, respectively. In Fig. 6(b), we find four branches around $\varepsilon/J_0 = 7$. These are spread when $|\Delta|$ is large, but they merge into a single line at $\Delta = 0$. The high-energy structure originates from the longitudinal modes of the local electric dipoles. In the case of the small anisotropy ($A/J_0 = 1$) in Fig. 6(a), we find the low-energy structure in addition to the high-energy branches. The energy increases linearly for the negative $\Delta$ region. Note that the low-energy structure is asymmetric for $\Delta$ while the high-energy one is symmetric. This is because the former originates from the transverse modes related to the $p$-orbital fluctuation, which is eliminated by the positive $\Delta$, but the latter originates from the excitation from the $s$ to $p$ orbital. In both cases, the lowest-energy part of $\Omega^{xy}(\varepsilon)$ is negative, leading to the positive $\beta^{xy}$. In the case of small anisotropy, the transverse modes exist at the lower energy, and therefore the large thermopolarization is observed in the vicinity of the phase boundary.

## V. DISCUSSION

Here, we estimate the magnitude of the off-diagonal thermopolarization in the present mechanism, and we discuss the emergence of the electric-toroidal dipole using the symmetry argument. First, we estimate the magnitude of the thermopolarization. We assume that the order of the local electric dipole $\boldsymbol{P}_i$ is scaled by $ea$, where $a$ is the length of the primitive translational vectors. Then, $\beta^{xy}$ should be scaled by $ek_B/aJ_0$. When $J_0 \sim 1$ meV, $\beta^{xy}$ is approximately given as the order of $10^{-10}$ C K$^{-1}$ m$^{-1}$. In this situation, the thermal gradient with $|\nabla T| \sim 1$ K/cm is expected to induce the electric polarization density with the order of $10^{-2}$ $\mu$C/m$^2$. It might be relatively small to observe the emergent polarization experimentally. However, since the polarization originating from the disproportionation of a local electronic cloud is often accompanied by the lattice distortion, we expect a more significant value of $\beta^{xy}$ in real materials. Moreover, the value might also be enhanced by increasing the thermal gradient and considering systems with smaller energy scales. This effect could be observed in the materials with the ferrotype electric-toroidal dipole order.

In the present setup, we can intuitively understand antisymmetric thermopolarization induced by the toroidal-type electric order in Fig. 1 as follows: When one applies the thermal gradient along the $y$ direction, the thermal fluctuations of the electric dipole moments at sites 2 and 4 are different, which leads to the macroscopic polarization along the $x$ direction. We provide here a general discussion on the appearance of antisymmetric thermopolarization using the symmetry argument. The present two-dimensional system on the square-octagon lattice belongs to the $D_{4h}$ symmetry. Under the symmetry, a time-reversal even $A_{2g}$ irreducible representation includes the components of electric-toroidal dipoles and electric hexadecapoles [27]. Nevertheless, the former should mainly participate in the thermopolarization coefficient because it is a rank-2 tensor. In general, only monopole, dipoles, and quadrupoles contribute to rank-2 linear-response tensors. Among them, electric-toroidal dipoles contribute to the antisymmetric part of the thermopolarization response tensor, but electric hexadecapoles do not. Therefore, the electric-toroidal dipole is crucial for antisymmetric thermopolarization, even in cases without isotropic symmetry. A similar argument has also been made in the context of the linear magnetoelectric effect, widely accepted in the community of multiferroics [31,69,70].

Here, we discuss the origin of the $A_{2g}$ irreducible representation of the $D_{4h}$ symmetry in the present system. Under this symmetry, the local $s$ and $p$ orbitals correspond to $A_{1g}$ and $E_u$, respectively, at each site. The local electronic degrees of freedom are represented by a $3 \times 3$ Hermitian matrix based on the real wave functions, the $s$, $p_x$, and $p_y$ orbitals, and it is decomposed by eight traceless matrices in addition to the unit matrix with the $A_{1g}$ symmetry. Note that five of them are real, and three are pure-imaginary matrices. The former are time-reversal even, and the latter are time-reversal odd. The local electronic degrees of freedom are decomposed into the following irreducible representations:

$$\begin{aligned}&(A_{1g}\oplus E_u)\otimes(A_{1g}\oplus E_u)\\ &\quad = 2A^+_{1g}\oplus A^-_{2g}\oplus B^+_{1g}\oplus B^+_{2g}\oplus E^+_u\oplus E^-_u,\end{aligned} \tag{19}$$

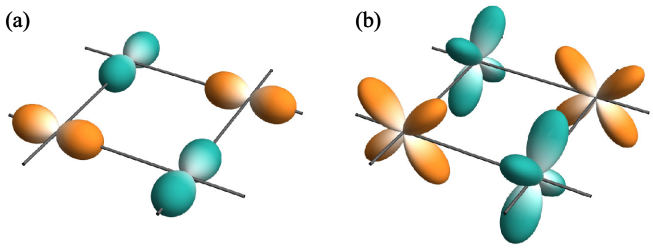


FIG. 7. Staggered-type orbital orders composed of (a) $p$ and (b) $d$ orbitals, which are expected to cause the antisymmetric thermopolarization.

where the suffix $+(-)$ denotes a time-reversal even (odd) representation. Among them, $E_u^+$ corresponds to the local electric dipole $\boldsymbol{P}_i = (P_i^x, P_i^y)$ at site $i$.

In addition to the local symmetry, we need to consider the symmetry of the four-sublattice structure. This degree of freedom is written as irreducible representations as follows:

$$A_{1g} \oplus B_{1g} \oplus E_u. \tag{20}$$

These correspond to sublattice modulations $(+,+,+,+)$ for $A_{1g}$, $(+,-,+,-)$ for $B_{1g}$, and $(+,0,-,0)$ and $(0,-,0,+)$ for $E_u$ in the labels of the sublattice, (1,2,3,4), presented in Fig. 1. The direct product of the irreducible representations in Eqs. (19) and (20) corresponds to the possible on-site four-sublattice order parameters. Here, we consider the direct product of $E_u^+$ in Eq. (19) and $E_u$ in Eq. (20), which is decomposed into $A_{1g}^+ \oplus A_{2g}^+ \oplus B_{1g}^+ \oplus B_{2g}^+$. In these irreducible representations, $A_{2g}^+$ corresponds to the electric-toroidal dipole. This is intuitively understood as follows: $P^y$ appearing with the sublattice modulation $(+,0,-,0)$ and $P^x$ appearing with $(0,-,0,+)$ correspond to the polarization arrangement shown in Fig. 1.

On the other hand, the $A_{2g}^+$ symmetry also appears in the direct product of $B_{2g}^+$ in Eq. (19) and $B_{1g}$ in Eq. (20). The $B_{2g}^+$ symmetry is derived from the direct product $E_u \otimes E_u$ within the $p$-orbital sector of the local electronic degrees of freedom, and $B_{1g}$ originates from the sublattice structure. This suggests that a simple staggered $p$ orbital order on a tetragonal (or square) lattice, which leads to the symmetry lowering from $D_{4h}$ to $C_{4h}$ in Fig. 7(a), also includes the component of an electric-toroidal dipole order. Moreover, under this $p$ orbital order, the antisymmetric off-diagonal thermopolarization should emerge if an $s$ orbital is present near the $p$ orbitals for nonzero matrix elements of the local polarization operator. This leads to a nonzero value of $\Omega_{\boldsymbol{kn}}^{xy}$ in Eq. (14) and the occurrence of antisymmetric thermopolarization in the present formalism. Indeed, we could introduce the electric polarization spanning a bond for neighboring sites, which is nonzero, even without the $s$ orbital. Thus, interacting $p$ models with the staggered orbital order at low temperatures have a potential to exhibit nonzero antisymmetric thermopolarization. Moreover, a similar argument can be made in $d$-orbital systems with local $E_g$ symmetry [see Fig. 7(b)], which will enlarge the range of candidate materials.

While the model addressed in the present study is somewhat artificial, we have discussed the magnitude of the antisymmetric thermopolarization and introduced more realistic orbital orders resulting in the thermopolarization using the symmetry argument. Since we have found that the antisymmetric thermopolarization is attributed to the appearance of the ferrotype electric-toroidal dipole order, the compounds with the ferroaxial order for lattice distortions potentially exhibit nonzero antisymmetric thermopolarization. The candidate materials are listed as $CaMn_7O_{12}$ [34], $NiTiO_3$ [53], $RbFe(MoO_4)_2$ [54], and $Ca_5Ir_3O_{12}$ [71]. It is desired to search other materials exhibiting electric-toroidal dipole orders in the electronic origin, which might be controllable via the degrees of freedom intrinsic to electrons, such as charge and spin. The candidates are not only transition-metal oxides but also organic salts.

Finally, we comment on an approach to distinguishing the antisymmetric part of $\beta^{xy}$ from its symmetric part, which is not addressed in the present study. The off-diagonal symmetric part is taken to be zero by rotating the coordinate axes such that the $2 \times 2$ matrix $\beta^{\mu\nu}$ $(\mu, \nu = x, y)$ is diagonalized. Even if the off-diagonal symmetric part is observed in real materials, we can vanish it by applying the thermal gradient along a high-symmetric crystal axis. This setup will be achieved by considering the crystal symmetry of the target material unless the crystal structure belongs to exceptionally low symmetries such as triclinic.

## VI. SUMMARY

In summary, we elucidated that the ferrotype electric-toroidal dipole order induces the antisymmetric thermopolarization by introducing a three-orbital model with $s$ and $p$ orbitals on a two-dimensional lattice. The mean-field theory suggests that this order emerges when the energy levels of the three local orbitals are close to each other. By taking account of the fluctuations from the mean fields, we calculate the antisymmetric part of the thermopolarization based on the linear-response theory. This quantity is strongly enhanced around the phase boundary, where the electric-toroidal dipole order disappears, and the $p$-orbital level is lower than that of the $s$ orbital. The low-energy spectrum clarifies that fluctuations of the $p$ orbitals are crucial for enhancing the thermopolarization. We also estimated the magnitude of the thermopolarization, and we discussed the origin based on the symmetry argument. The present results suggest that the thermal gradient can unveil the electric-toroidal dipole order as a linear response and stimulate further investigations on the electric toroidicity in materials. On the other hand, our model might be too simple to compare the real compounds directly. A more realistic model is desired to be proposed, but it is a future issue.

## ACKNOWLEDGMENTS

The authors thank H. Kusunose for fruitful discussions. Parts of the numerical calculations were performed in the supercomputing systems in ISSP, the University of Tokyo. This work was supported by Grant-in-Aid for Scientific Research from JSPS, KAKENHI Grants No. JP19K03752, No. JP19K03742, No. JP20H00122, No. JP21H01037, No. JP22H04468, No. JP22H01183, and by JST PRESTO (JPMJPR19L5 and JPMJPR20L8).

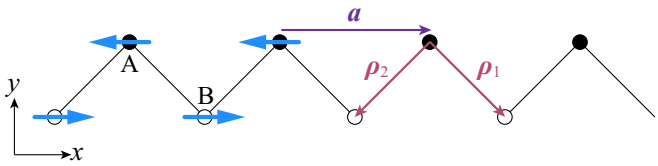


FIG. 8. Schematic picture of the zigzag lattice on which the transverse Ising model is defined. The blue arrows represent the electric dipole moments, which exhibit a staggard-type ordering along the $x$ direction. $\boldsymbol{a}$ is the primitive translational vector, and $\boldsymbol{\rho}_1$ and $\boldsymbol{\rho}_2$ are the vectors connecting between neighboring sites.

## APPENDIX: TRANSVERSE ISING MODEL ON A ZIGZAG CHAIN

In this Appendix, we consider the transverse Ising model on a zigzag lattice as one of the simplest models exhibiting electric-toroidal dipole order. The Hamiltonian is written as

$$\mathcal{H}_{\rm TI} = J\sum_{\langle ij\rangle}\sigma_i^x\sigma_j^x - \Gamma\sum_i \sigma_i^z, \tag{A1}$$

where $\sigma_i^x$ and $\sigma_i^z$ are the Pauli matrices for two local bases with different parity at site $i$, and the antiferrotype interaction with $J > 0$ is assumed. We regard $\sigma_i^x$ as a local electric dipole along the $x$ direction, which appears by mixing the two local states. This means that the two local bases are given by $s$ and $p_x$ orbitals. The first term means the interactions between electric dipoles, and the second term represents the level splitting, which suppresses the electric dipole moment.

Here, we apply the two-sublattice mean-field approximation to Eq. (A1), where the two types of local moments are given as

$$-\langle\sigma^x\rangle_A = \langle\sigma^x\rangle_B \equiv X, \tag{A2}$$

$$\langle\sigma^z\rangle \equiv Z, \tag{A3}$$

where we assume the staggered order shown in Fig. 8 for the $A$ and $B$ sublattices when $X \neq 0$. In this case, the mean-field energy is given by

$$E_{\rm MF}/N = -JX^2 - \Gamma Z, \tag{A4}$$

and the mean-field solution is obtained as

$$\begin{aligned} &Z = \Gamma/\Gamma_c, \quad X = \sqrt{1-Z^2} \quad \text{for } |\Gamma| \leqslant \Gamma_c, \\ &Z = \mathrm{sgn}(\Gamma), \quad X = 0 \quad\quad\ \text{for } |\Gamma| > \Gamma_c, \end{aligned} \tag{A5}$$

where $\Gamma_c$ is the critical field given by $\Gamma_c = 2J$.

The elementary excitations from the mean-field ground state are described by bosons as

$$\begin{aligned} \mathcal{H} \simeq \tilde{\mathcal{H}} = E_{\rm MF} + \Delta E\sum_i a_i^\dagger a_i - JZ^2 \\ \times\sum_{\langle ij\rangle}(a_i^\dagger a_j + a_i a_j + \text{H.c.}), \end{aligned} \tag{A6}$$

where $\Delta E = 4JX^2 + 2\Gamma Z$. By applying the Fourier transformation given as

$$a_i = \begin{cases} \sqrt{\frac{2}{N}}\sum_k a_k e^{i\boldsymbol{k}\cdot\boldsymbol{r}_i} & \text{for } i \in A, \\ \sqrt{\frac{2}{N}}\sum_k b_k e^{i\boldsymbol{k}\cdot\boldsymbol{r}_i} & \text{for } i \in B, \end{cases} \tag{A7}$$

the low-energy Hamiltonian is represented as

$$\tilde{\mathcal{H}} = E_{\rm MF} - \frac{\Delta EN}{2} + \frac{1}{2}\sum_{\boldsymbol{k}}\mathcal{A}_{\boldsymbol{k}}^\dagger H_{\boldsymbol{k}}\mathcal{A}_{\boldsymbol{k}}, \tag{A8}$$

where $\mathcal{A}_{\boldsymbol{k}} = (a_{\boldsymbol{k}}, b_{\boldsymbol{k}}, a_{-\boldsymbol{k}}^\dagger, b_{-\boldsymbol{k}}^\dagger)^T$ and $J_{\boldsymbol{k}} = -JZ^2\sum_{\gamma=1,2} e^{i\boldsymbol{k}\cdot\boldsymbol{\rho}_\gamma}$ with $\boldsymbol{\rho}_1 = (1/2, -1.2)$ and $\boldsymbol{\rho}_2 = (-1/2, -1.2)$. The Hamiltonian matrix $H_{\boldsymbol{k}}$ is given by

$$H_{\boldsymbol{k}} = \begin{pmatrix} \Delta E & J_{\boldsymbol{k}} & 0 & J_{\boldsymbol{k}} \\ J_{\boldsymbol{k}}^* & \Delta E & J_{\boldsymbol{k}}^* & 0 \\ 0 & J_{\boldsymbol{k}} & \Delta E & J_{\boldsymbol{k}} \\ J_{\boldsymbol{k}}^* & 0 & J_{\boldsymbol{k}}^* & \Delta E \end{pmatrix}. \tag{A9}$$

This matrix is diagonalized by applying the Bogoliubov transformation with paraunitary matrix $T_{\boldsymbol{k}}$, and the energies of the two corrective modes are calculated as

$$\varepsilon_{\boldsymbol{k}}^{\pm} = \sqrt{\Delta E(\Delta E \pm 2|J_{\boldsymbol{k}}|)}. \tag{A10}$$

The velocity defined in Eq. (12) is represented as

$$\mathcal{V}_{\boldsymbol{k}}^y = T_{\boldsymbol{k}}^\dagger\frac{\partial H_{\boldsymbol{k}}}{\partial k_y}T_{\boldsymbol{k}} = -\frac{i\Delta E|J_{\boldsymbol{k}}|}{2\sqrt{\varepsilon_{\boldsymbol{k}}^+\varepsilon_{\boldsymbol{k}}^-}}\begin{pmatrix} & 1 & & 1 \\ -1 & & -1 & \\ & 1 & & 1 \\ -1 & & -1 & \end{pmatrix}. \tag{A11}$$

Moreover, we introduce the polarization defined by

$$P^x = \sum_i \sigma_i^x. \tag{A12}$$

This is rewritten by using the bosons and is approximately given by

$$P^x \simeq 2X\sum_{\boldsymbol{k}}(a_{\boldsymbol{k}}^\dagger a_{\boldsymbol{k}} - b_{\boldsymbol{k}}^\dagger b_{\boldsymbol{k}}) = \frac{1}{2}\sum_{\boldsymbol{k}}\mathcal{A}_{\boldsymbol{k}}^\dagger P_{\boldsymbol{k}}^x\mathcal{A}_{\boldsymbol{k}}, \tag{A13}$$

where we neglect the linear terms of bosonic operators as they change the parity of the number of bosons. $P_{\boldsymbol{k}}^x$ is a $4\times 4$ matrix given as

$$P_{\boldsymbol{k}}^x = \begin{pmatrix} 2X & & & \\ & -2X & & \\ & & 2X & \\ & & & -2X \end{pmatrix}. \tag{A14}$$

The matrix $\mathcal{P}_{\boldsymbol{k}}^x$ defined in Eq. (11) is evaluated by $\mathcal{P}_{\boldsymbol{k}}^x = T_{\boldsymbol{k}}^\dagger P_{\boldsymbol{k}}^x T_{\boldsymbol{k}}$. Using the representations of $\mathcal{V}_{\boldsymbol{k}}^y$ and $\mathcal{P}_{\boldsymbol{k}}^x$, we can calculate $\Omega_{\boldsymbol{k}\pm}^{xy}$ in Eq. (14) as

$$\Omega_{\boldsymbol{k}\pm}^{xy} = \pm\frac{X}{2|J_{\boldsymbol{k}}|}. \tag{A15}$$

Thus, the coefficient of the transverse thermopolarization, $\beta^{xy}$, is represented as

$$\beta^{xy} = \frac{1}{V}\sum_{\boldsymbol{k}}\frac{X}{2|J_{\boldsymbol{k}}|}\{c_1(n(\varepsilon_{\boldsymbol{k}}^-)) - c_1(n(\varepsilon_{\boldsymbol{k}}^+))\}. \tag{A16}$$

Figure 9 shows the $\Gamma$ dependence of $\beta^{xy}$. We find that $\beta^{xy}$ is an even function of $\Gamma$ and increases with increasing temperature. Moreover, this quantity is enhanced around the critical points $\Gamma/J = \pm 2$, but it takes a small value compared to the

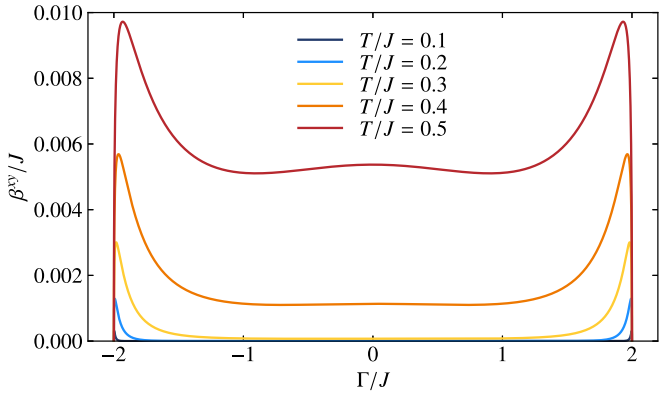


FIG. 9. The transverse field dependence of $\beta^{xy}$ in the transverse Ising model on a zigzag lattice at several temperatures. We assume that the volume of the unit cell is unity.

energy scale of $J$. The behavior of $\beta^{xy}$ is distinctly different from that in the three-orbital model on the square-octagon lattice, which is shown in Fig. 3(b), while $\langle G \rangle$ as a function of $\Delta$ shown in Fig. 3(a) is similar to the $\Gamma$ dependence of the ordered moment $X$ given in Eq. (A2), where $X = \sqrt{1 - \Gamma^2/\Gamma_c^2}$ in the ordered phase with $|\Gamma| < \Gamma_c$.

Finally, we discuss the appearance of the electric-toroidal dipole order in the transverse Ising model on the zigzag chain from the viewpoint of the symmetry. Under the $D_{2h}$ symmetry, the localized $s$ and $p_x$ orbitals belong to $A_g$ and $B_{3u}$. Then, the local electronic degrees of freedom are given by the $2 \times 2$ matrix, which is decomposed into $2A_g^+ \oplus B_{3u}^+ \oplus B_{3u}^-$. The sublattice degree of freedom is described as $A_g \oplus B_{2u}$. The $z$ component of the electric-toroidal dipole moment belongs to $B_{1g}^+$, which appears as a part of the direct product of $B_{3u}^+$ in the former and $B_{2u}$ in the latter.


[1] P. Curie, Sur la symétrie dans les phénomènes physiques, symétrie d'un champ électrique et d'un champ magnétique, J. Phys. Theor. Appl. **3**, 393 (1894).

[2] I. E. Dzyaloshinskiĭ, On the magneto-electrical effects in antiferromagnets, Sov. Phys. JETP **10**, 628 (1960).

[3] D. Astrov, The magnetoelectric effect in antiferromagnetics, Sov. Phys. JETP **11**, 708 (1960).

[4] V. J. Folen, G. T. Rado, and E. W. Stalder, Anisotropy of the Magnetoelectric Effect in $Cr_2O_3$, Phys. Rev. Lett. **6**, 607 (1961).

[5] T. Kimura, T. Goto, H. Shintani, K. Ishizaka, T.-H. Arima, and Y. Tokura, Magnetic control of ferroelectric polarization, Nature (London) **426**, 55 (2003).

[6] M. Fiebig, Revival of the magnetoelectric effect, J. Phys. D **38**, R123 (2005).

[7] H. Katsura, N. Nagaosa, and A. V. Balatsky, Spin Current and Magnetoelectric Effect in Noncollinear Magnets, Phys. Rev. Lett. **95**, 057205 (2005).

[8] D. I. Khomskii, Multiferroics: Different ways to combine magnetism and ferroelectricity, J. Magn. Magn. Mater. **306**, 1 (2006).

[9] S.-W. Cheong and M. Mostovoy, Multiferroics: A magnetic twist for ferroelectricity, Nat. Mater. **6**, 13 (2007).

[10] D. Khomskii, Trend: Classifying multiferroics: Mechanisms and effects, Physics **2**, 20 (2009).

[11] C. Wang and M. Pang, Thermally induced spin polarization and thermal conductivities in a spin–orbit-coupled two-dimensional electron gas, Solid State Commun. **150**, 1509 (2010).

[12] A. Dyrdał, M. Inglot, V. K. Dugaev, and J. Barnaś, Thermally induced spin polarization of a two-dimensional electron gas, Phys. Rev. B **87**, 245309 (2013).

[13] C. Xiao, D. Li, and Z. Ma, Thermoelectric response of spin polarization in Rashba spintronic systems, Front. Phys. **11**, 117201 (2016).

[14] A. Dyrdał, J. Barnaś, V. K. Dugaev, and J. Berakdar, Thermally induced spin polarization in a magnetized two-dimensional electron gas with Rashba spin-orbit interaction, Phys. Rev. B **98**, 075307 (2018).

[15] A. Shitade, A. Daido, and Y. Yanase, Theory of spin magnetic quadrupole moment and temperature-gradient-induced magnetization, Phys. Rev. B **99**, 024404 (2019).

[16] M. Marvan, The electric polarization induced by temperature gradient and associated thermoelectric effects, Czech. J. Phys. B **19**, 1240 (1969).

[17] V. L. Gurevich, Electrothermal effect in crystalline insulators, Sov. Phys. Solid State **23**, 1377 (1981).

[18] A. L. Kholkin, V. A. Trepakov, and G. A. Smolenskĭ, Thermopolarization currents in dielectrics, JETP Lett. **35**, 124 (1982).

[19] V. L. Gurevich and A. K. Tagantsev, Theory for the thermopolarization effect in dielectrics having a center of inversion, JETP Lett. **35**, 128 (1982).

[20] V. A. Trepakov, K. M. Nurieva, and A. K. Tagantsev, Recent developments of the thermopolarization effect investigation, Ferroelectrics **94**, 377 (1989).

[21] K. M. Nurieva, A. K. Tagantsev, V. A. Trepakov, and V. M. Varikash, Observation of thermal polarization effect in piezoelectrics (kdp), Fiz. Tverd. Tela **31**, 130 (1989).

[22] A. K. Tagantsev, Electric polarization in crystals and its response to thermal and elastic perturbations, Phase Trans. **35**, 119 (1991).

[23] V. A. Trepakov, E. T. Rafikov, M. Marvan, L. Jastrabik, and N. P. Divin, Observation of the "dielectric peltier effect," Europhys. Lett. **21**, 891 (1993).

[24] F. Bresme, A. Lervik, D. Bedeaux, and S. Kjelstrup, Water Polarization under Thermal Gradients, Phys. Rev. Lett. **101**, 020602 (2008).

[25] P. Wirnsberger, C. Dellago, D. Frenkel, and A. Reinhardt, Theoretical Prediction of Thermal Polarization, Phys. Rev. Lett. **120**, 226001 (2018).

[26] Y. Onishi, H. Isobe, and N. Nagaosa, Theory of thermoelectric effect in insulators, arXiv:2105.08228.

[27] S. Hayami, M. Yatsushiro, Y. Yanagi, and H. Kusunose, Classification of atomic-scale multipoles under crystallographic point groups and application to linear response tensors, Phys. Rev. B **98**, 165110 (2018).

[28] M.-T. Suzuki, H. Ikeda, and P. M. Oppeneer, First-principles theory of magnetic multipoles in condensed matter systems, J. Phys. Soc. Jpn. **87**, 041008 (2018).

[29] H. Watanabe and Y. Yanase, Group-theoretical classification of multipole order: Emergent responses and candidate materials, Phys. Rev. B **98**, 245129 (2018).

[30] M. Yatsushiro, H. Kusunose, and S. Hayami, Multipole classification in 122 magnetic point groups for unified understanding of multiferroic responses and transport phenomena, Phys. Rev. B **104**, 054412 (2021).

[31] N. A. Spaldin, M. Fiebig, and M. Mostovoy, The toroidal moment in condensed-matter physics and its relation to the magnetoelectric effect, J. Phys.: Condens. Matter **20**, 434203 (2008).

[32] Y. V. Kopaev, Toroidal ordering in crystals, Phys. Usp. **52**, 1111 (2009).

[33] V. Dubovik and V. Tugushev, Toroid moments in electrodynamics and solid-state physics, Phys. Rep. **187**, 145 (1990).

[34] R. D. Johnson, L. C. Chapon, D. D. Khalyavin, P. Manuel, P. G. Radaelli, and C. Martin, Giant Improper Ferroelectricity in the Ferroaxial Magnet $CaMn_7O_{12}$, Phys. Rev. Lett. **108**, 067201 (2012).

[35] J. Hlinka, J. Privratska, P. Ondrejkovic, and V. Janovec, Symmetry Guide to Ferroaxial Transitions, Phys. Rev. Lett. **116**, 177602 (2016).

[36] S.-W. Cheong, D. Talbayev, V. Kiryukhin, and A. Saxena, Broken symmetries, non-reciprocity, and multiferroicity, npj Quantum Mater. **3**, 19 (2018).

[37] S. Hayami and H. Kusunose, Microscopic description of electric and magnetic toroidal multipoles in hybrid orbitals, J. Phys. Soc. Jpn. **87**, 033709 (2018).

[38] M. Hanawa, Y. Muraoka, T. Tayama, T. Sakakibara, J. Yamaura, and Z. Hiroi, Superconductivity at 1 K in $Cd_2Re_2O_7$, Phys. Rev. Lett. **87**, 187001 (2001).

[39] R. Jin, J. He, S. McCall, C. S. Alexander, F. Drymiotis, and D. Mandrus, Superconductivity in the correlated pyrochlore $Cd_2Re_2O_7$, Phys. Rev. B **64**, 180503(R) (2001).

[40] Z. Hiroi, T. Yamauchi, T. Yamada, M. Hanawa, Y. Ohishi, O. Shimomura, M. Abliz, M. Hedo, and Y. Uwatoko, High-pressure study on the superconducting pyrochlore oxide $Cd_2Re_2O_7$, J. Phys. Soc. Jpn. **71**, 1553 (2002).

[41] J.-I. Yamaura and Z. Hiroi, Low temperature symmetry of pyrochlore oxide $Cd_2Re_2O_7$, J. Phys. Soc. Jpn. **71**, 2598 (2002).

[42] J. P. Castellan, B. D. Gaulin, J. van Duijn, M. J. Lewis, M. D. Lumsden, R. Jin, J. He, S. E. Nagler, and D. Mandrus, Structural ordering and symmetry breaking in $Cd_2Re_2O_7$, Phys. Rev. B **66**, 134528 (2002).

[43] C. A. Kendziora, I. A. Sergienko, R. Jin, J. He, V. Keppens, B. C. Sales, and D. Mandrus, Goldstone-Mode Phonon Dynamics in the Pyrochlore $Cd_2Re_2O_7$, Phys. Rev. Lett. **95**, 125503 (2005).

[44] N. Barišić, L. Forró, D. Mandrus, R. Jin, J. He, and P. Fazekas, Electrical properties of $Cd_2Re_2O_7$ under pressure, Phys. Rev. B **67**, 245112 (2003).

[45] I. A. Sergienko and S. H. Curnoe, Structural order parameter in the pyrochlore superconductor $Cd_2Re_2O_7$, J. Phys. Soc. Jpn. **72**, 1607 (2003).

[46] T. C. Kobayashi, Y. Irie, J.-i. Yamaura, Z. Hiroi, and K. Murata, Superconductivity of heavy carriers in the pressure-induced phases of $Cd_2Re_2O_7$, J. Phys. Soc. Jpn. **80**, 023715 (2011).

[47] J.-i. Yamaura, K. Takeda, Y. Ikeda, N. Hirao, Y. Ohishi, T. C. Kobayashi, and Z. Hiroi, Successive spatial symmetry breaking under high pressure in the spin-orbit-coupled metal $Cd_2Re_2O_7$, Phys. Rev. B **95**, 020102(R) (2017).

[48] Z. Hiroi, J.-I. Yamaura, T. C. Kobayashi, Y. Matsubayashi, and D. Hirai, Pyrochlore oxide superconductor $Cd_2Re_2O_7$ revisited, J. Phys. Soc. Jpn. **87**, 024702 (2018).

[49] Y. Matsubayashi, D. Hirai, M. Tokunaga, and Z. Hiroi, Formation and control of twin domains in the pyrochlore oxide $Cd_2Re_2O_7$, J. Phys. Soc. Jpn. **87**, 104604 (2018).

[50] S. Di Matteo and M. R. Norman, Nature of the tensor order in $Cd_2Re_2O_7$, Phys. Rev. B **96**, 115156 (2017).

[51] S. Hayami, Y. Yanagi, H. Kusunose, and Y. Motome, Electric Toroidal Quadrupoles in the Spin-Orbit-Coupled Metal $Cd_2Re_2O_7$, Phys. Rev. Lett. **122**, 147602 (2019).

[52] S. Hayami, R. Oiwa, and H. Kusunose, Electric ferro-axial moment as nanometric rotator and source of longitudinal spin current, arXiv:2111.10519.

[53] T. Hayashida, Y. Uemura, K. Kimura, S. Matsuoka, D. Morikawa, S. Hirose, K. Tsuda, T. Hasegawa, and T. Kimura, Visualization of ferroaxial domains in an order-disorder type ferroaxial crystal, Nat. Commun. **11**, 4582 (2020).

[54] W. Jin, E. Drueke, S. Li, A. Admasu, R. Owen, M. Day, K. Sun, S.-W. Cheong, and L. Zhao, Observation of a ferro-rotational order coupled with second-order nonlinear optical fields, Nat. Phys. **16**, 42 (2020).

[55] P. de Gennes, Collective motions of hydrogen bonds, Solid State Commun. **1**, 132 (1963).

[56] J. Hemberger, M. Nicklas, R. Viana, P. Lunkenheimer, A. Loidl, and R. Böhmer, Quantum paraelectric and induced ferroelectric states, J. Phys.: Condens. Matter **8**, 4673 (1996).

[57] S. A. Prosandeev, W. Kleemann, B. Westwański, and J. Dec, Quantum paraelectricity in the mean-field approximation, Phys. Rev. B **60**, 14489 (1999).

[58] F. P. Onufrieva, Low-temperature properties of spin systems with tensor order parameters, Zh. Eksp. Teor. Fiz **89**, 2270 (1985).

[59] N. Papanicolaou, Unusual phases in quantum spin-1 systems, Nucl. Phys. B **305**, 367 (1988).

[60] H. Kusunose and Y. Kuramoto, Spin-orbital wave excitations in orbitally degenerate exchange model with multipolar interactions, J. Phys. Soc. Jpn. **70**, 3076 (2001).

[61] R. Shiina, H. Shiba, P. Thalmeier, A. Takahashi, and O. Sakai, Dynamics of multipoles and neutron scattering spectra in quadrupolar ordering phase of $CeB_6$, J. Phys. Soc. Jpn. **72**, 1216 (2003).

[62] A. Joshi, M. Ma, F. Mila, D. N. Shi, and F. C. Zhang, Elementary excitations in magnetically ordered systems with orbital degeneracy, Phys. Rev. B **60**, 6584 (1999).

[63] Y. Murakami, T. Oka, and H. Aoki, Supersolid states in a spin system: Phase diagram and collective excitations, Phys. Rev. B **88**, 224404 (2013).

[64] J. Nasu and S. Ishihara, Vibronic excitation dynamics in orbitally degenerate correlated electron system, Phys. Rev. B **88**, 205110 (2013).

[65] J. H. P. Colpa, Diagonalization of the quadratic boson hamiltonian, Physica A **93**, 327 (1978).

[66] S. Murakami and A. Okamoto, Thermal hall effect of magnons, J. Phys. Soc. Jpn. **86**, 011010 (2017).

[67] A. Shitade and Y. Yanase, Magnon gravitomagnetoelectric effect in noncentrosymmetric antiferromagnetic insulators, Phys. Rev. B **100**, 224416 (2019).

[68] B. Li, A. Mook, A. Raeliarijaona, and A. A. Kovalev, Magnonic analog of the Edelstein effect in antiferromagnetic insulators, Phys. Rev. B **101**, 024427 (2020).

[69] H. Schmid, Some symmetry aspects of ferroics and single phase multiferroics, J. Phys.: Condens. Matter **20**, 434201 (2008).

[70] N. A. Spaldin and R. Ramesh, Advances in magnetoelectric multiferroics, Nat. Mater. **18**, 203 (2019).

[71] H. Hanate, T. Hasegawa, S. Hayami, S. Tsutsui, S. Kawano, and K. Matsuhira, First observation of superlattice reflections in the hidden order at 105 K of spin-orbit coupled iridium oxide $Ca_5Ir_3O_{12}$, J. Phys. Soc. Jpn. **90**, 063702 (2021).